Novel nitride quantum structures for infrared sensing

Oana Malis,[1,*] Trang Nguyen,[1] Yang Cao,[1] Brenden A. Magill,[2] Brandon Dzuba,[1,3] Stephen McGill,[4] Carlos Garcia,[4,5] Giti A. Khodaparast, Michael J. Manfra,[1,3,6,7]

[1]Department of Physics and Astronomy, Purdue University, West Lafayette, Indiana 47907, USA
[2]Department of Physics, Virginia Tech, Blacksburg, VA, 24061, USA
[3]Birck Nanotechnology Center, Purdue University, West Lafayette, Indiana 47907, USA
[4]National High Magnetic Field Laboratory, Tallahassee, FL 32310, USA
[5]Department of Physics, Florida State University, Tallahassee, FL 32306, USA
[6]Elmore Family School of Electrical and Computer Engineering, Purdue University, West Lafayette, Indiana 47907, USA
[7]School of Materials Engineering, Purdue University, West Lafayette, Indiana 47907, USA
*omalis@purdue.edu

ABSTRACT

Band structure, strain, and polarization engineering of nitride heterostructures open unparalleled opportunities for quantum sensing in the infrared. Intersubband absorption and photoluminescence are employed to correlate structure with optical properties of nonpolar strain-balanced InGaN/AlGaN nanostructures grown by molecular-beam epitaxy. Mid-infrared intersubband transitions in m-plane (In)$Al_xGa_{1-x}N/In_{0.16}Ga_{0.84}N$ ($0.19 \leq x \leq 0.3$) multi-quantum wells were observed for the first time in the range of 3.4-5.1 μm (244-360 meV). Direct and attenuated total-reflection infrared absorption measurements are interpreted using structural information revealed by high-resolution x-ray diffraction and transmission electron microanalysis. The experimental intersubband energies are better reproduced by calculations using the local-density approximation than the Hartree-Fock approximation for the exchange-correlation correction. The effect of charge density, quantum well width, and barrier alloy composition on the intersubband transition energy was examined to evaluate the potential of this material for practical infrared applications.

Temperature-dependent continuous-wave and time-resolved photoluminescence (TRPL) measurements are also investigated to probe carrier localization and recombination in m-plane InGaN/AlGaN quantum wells. Average localization depths of 21 meV and 40 meV were estimated for the undoped and doped structures, respectively. Using TRPL, dual localization centers were identified in undoped structures, while a single type of localization centers was found in doped structures. At 2 K, a fast decay time of approximately 0.3ns was measured for both undoped and doped structures, while a longer decay time of 2.2 ns was found only for the undoped sample. TRPL in magnetic field was explored to examine the effect of doping sheets on carrier dynamics.

Keywords: nitride semiconductors, intersubband absorption, photoluminescence

1. INTRODUCTION

The nitride semiconductors, best known for their applications in visible light-emitting diodes (LEDs) and power electronics,[1-4] also have the potential to enable quantum sensing in the infrared.[5-8] The large conduction band offset (CBO) and large longitudinal-optical (LO) phonon energy (90 meV) available for III-N heterostructures make possible quantum confinement in the conduction band and consequently intersubband (ISB) transitions spanning the near-infrared and far-infrared ranges currently inaccessible with other semiconductor materials. Fig. 1 shows schematically the infrared ranges targeted by nitride ISB lasers and detectors. Progress towards nitride ISB optoelectronic devices has been slowed so far by challenges related to practically achievable structural quality and fundamental material properties. The commercial availability of low-defect nitride substrates has considerably improved the quality outlook for nitride epitaxy. However, challenges remain due to lattice-mismatch and vastly different optimal growth conditions of Al- and In-containing alloys. Moreover, the built-in polarization fields endemic to the typical c-axis growth direction substantially limit design space for ISB devices. To overcome these challenges, we are investigating non-polar m-plane

strain-balanced InGaN/(In)AlGaN multi-quantum wells. This paper presents a study of the optical properties of these heterostructures in the visible and infrared ranges of the spectrum. ISB absorption and visible photoluminescence are employed to evaluate the impact of nanostructure on optical properties and to identify most adequate theoretical models to predict optical properties.

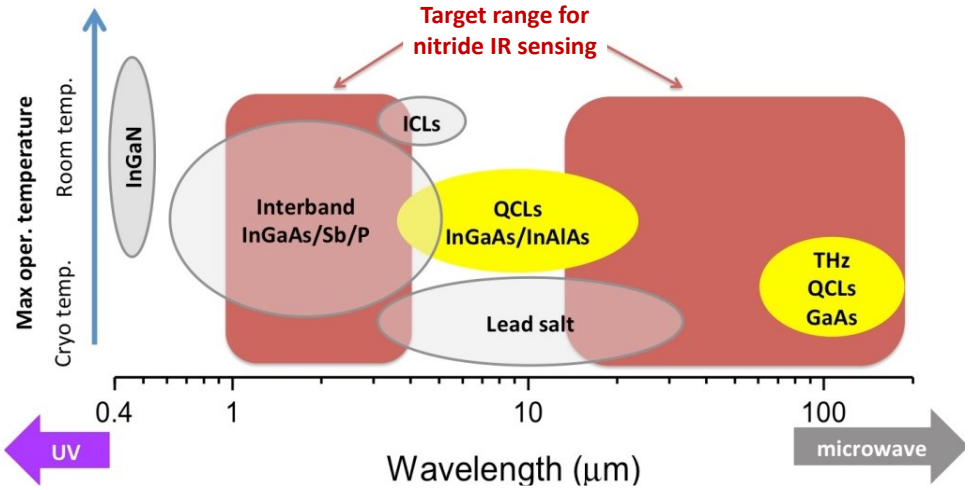

Figure 1. Target infrared ranges for nitride ISB optoelectronics.

2. EXPERIMENTAL AND CALCULATION DETAILS

All samples discussed in this paper consist of multiple InGaN quantum wells (QWs) with AlGaN barriers (also referred to as superlattices) grown by plasma-assisted molecular beam epitaxy (PAMBE). We take advantage of extensive material research in growing nitride heterostructures by molecular beam epitaxy.[9-18] The details of the growth process are given elsewhere.[17,18] Briefly, the PAMBE system is equipped with conventional effusion cells for indium, gallium, aluminum, and silicon. The active nitrogen flux was supplied by a Veeco Unibulb radio-frequency plasma source operated at 300 W forward power with 0.5 sccm of nitrogen (N_2) flow. The superlattices were grown at 565°C on commercially available non-polar m-plane (10-10) semi-insulating GaN substrates from Nanowin, Inc. The 5×10 mm^2 substrates are miscut -0.5° ± 0.2° towards the c-axis, have a surface root-mean-square roughness of less than 0.3 nm over 16 μm^2, and nominal threading dislocation density of less than 5×10^6 cm^{-2}.

The well and barrier thicknesses were chosen to minimize strain accumulation while keeping the Al composition in the barriers low enough to avoid aluminum segregation. The thickness-weighted method was used to approximate strain-balanced conditions: $\varepsilon_b t_b+\varepsilon_w t_w = 0$, where ε_b and ε_w represent the strain in the barrier and well, respectively, while t_b and t_w represent their respective layer thicknesses. Note that strain is anisotropic on the m-plane surface, and thus cannot be exactly balanced along both the a-axis and c-axis simultaneously. Therefore, the barrier and QW thicknesses were chosen so that strain is roughly balanced along the a-direction and there is less than 0.3% residual strain per period along the c-direction. The samples are either undoped or δ-doped in the barriers with two sheets of silicon located ~1 nm away from each barrier/QW interface.[19] The density of dopant of about 2×10^{14} cm^{-2} results in a calculated electron density of 8.6×10^{12} cm^{-2} in each QW.

The samples were characterized with high-resolution x-ray diffraction (HRXRD). ω-2θ spectra were collected by a PANalytical X'Pert-MRD high-resolution x-ray diffractometer equipped with a 4-bounce Ge monochromator. In order to extract layer thicknesses and alloy compositions, the software package Epitaxy 4.5a from PANalytical was used to simulate the HRXRD diffraction patterns. Structural data from HRXRD was confirmed with high-resolution high-angle annular dark field scanning transmission electron microscopy (HRHAADF-STEM) as shown for a set of representative samples in Fig. 2. HRHAADF-STEM images were taken with an aberration-corrected Thermo Scientific Themis Z microscope using a voltage of 300 kV, current of 0.24 nA, and 0.65 Å probe size. This microscope allows the images to be corrected up to the 3rd order of aberration including astigmatism, spherical, coma, etc.

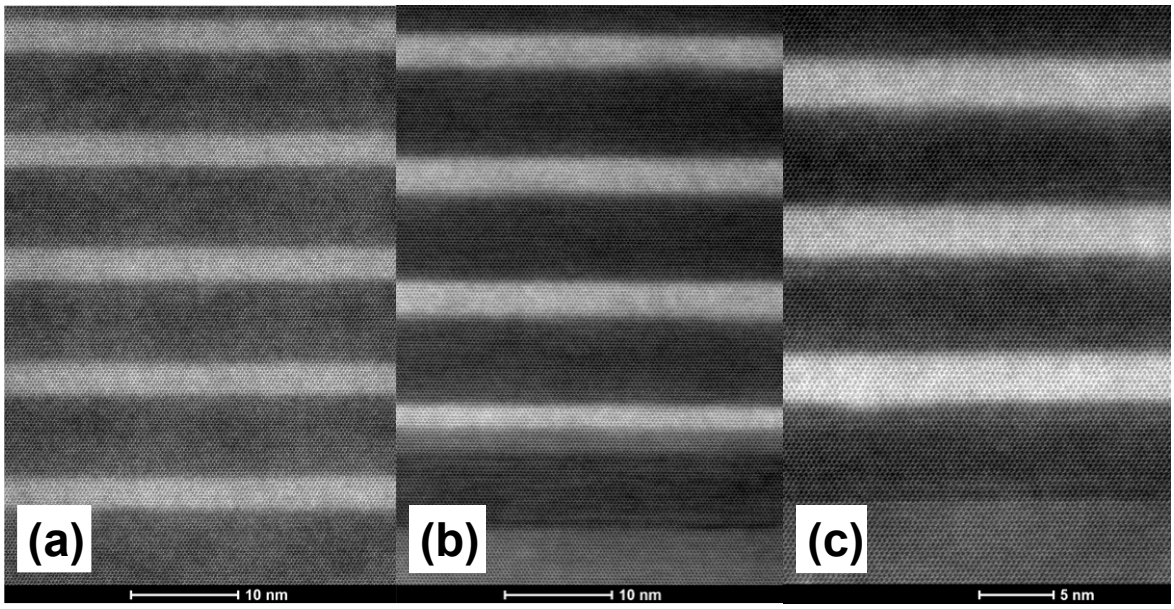

Figure 2. HRHAADF-STEM image of m-plane InGaN/AlGaN multi-QW samples A (a), B (b), and C (c) with the structural parameters listed in the table shown in Fig. 2.

A combination of direct Fourier transform infrared (FTIR) spectroscopy and attenuated total reflectance FTIR (ATR-FTIR) is used to perform ISB absorption (ISBA) measurements on all samples using a Thermo Scientific Nicolet 8700 spectrometer (Fig. 3(a-c)).[19] For direct FTIR measurements, sample preparation involved cleaving samples to small pieces and polishing 45° facets on both sides. In some cases, a gold film was deposited on top of the active region to enhance ISBA intensity. For the ATR-FTIR method, the samples were sandwiched with a polished Ge crystal to allow an evanescent wave to probe absorption in the MQW stack (Fig. 3(a)). This technique is ideal for measuring ISBA in the range where the substrate is opaque. However, as the specimen is squeezed against the Ge crystal, an unintentional air gap between the interfaces may affect the penetration depth of the evanescent wave, and hence, the absorption intensity. Therefore, quantitative results by this technique are sometimes affected by experimental artifacts. The ISBA spectra were obtained by first normalizing the p- and s-polarized transmission spectra to the backgrounds, and then taking the ratio of the p- to the s-polarized spectra. For the ATR-FTIR, the backgrounds were collected in transmission through the Ge crystal without any sample.

The photoluminescence (PL) measurements were performed on m-plane superlattices consisting of 15 $In_{0.09}Ga_{0.91}N$ QWs with $Al_{0.19}Ga_{0.81}N$ barriers grown by PAMBE. The continuous excitation PL experiments utilized a 325 nm cw He-Cd laser with excitation power of about 10 mW, corresponding to an estimated excitation carrier density of 6.3×10^{11} cm^{-3}. This is weak excitation which does not significantly affect the band structure.[33,34] The samples were placed in a liquid helium flow cryostat and measured in reflection geometry in the range from 8 K to room temperature. The PL spectra were collected by a Cary Eclipse Fluorescence Spectrometer equipped with a photomultiplier tube. We corrected the spectra by subtracting a linear background and fitting with a Gaussian function to extract the transition energy and full-width-at-half-maximum (FWHM).

Time-resolved photoluminescence (TRPL) was measured in a helium flow-through cryostat from 2 to 100 K. In our measurements we used femtosecond 784 nm pulses which were upconverted to 384 nm, using a non-linear crystal (BBO) generating an average power of ~ 80μW. The pulses were produced by a Mira 900 Ti:sapphire oscillator with a repetition rate of 80 MHz. Light emitted at the PL peak (~408 nm) was selected using a monochromator then collected from the sample in a reflectivity geometry, using an avalanche photodiode. A Faraday geometry was used in magnetic field dependence TRPL measurements, where the direction of the field is perpendicular to the epilayer plane. A time correlated single photon counting system (Picoharp 300) was used to determine the time between excitation pulse and emission of PL photons.

The nextnano++ software package was used to calculate the electronic band structure of single QWs using the 8-band **k·p** model and the structural parameters from HRXRD and HRHAADF-STEM.[20] The program solves the Schrödinger and Poisson equations self-consistently to estimate the electronic energy levels and the amount of activated charge inside each QW using generally accepted nitride material parameters.[21] The IBS transition energies were corrected for many-body effects including exchange-correlation, depolarization, and excitonic corrections.[22-24] The exchange-correlation correction was estimated following two different approaches: the Hartree-Fock approximation (HFA) and the local density approximation (LDA).[25-28] The interband transition energies were adjusted to include the exciton binding energy.[29]

3. INTERSUBBAND ABSORPTION

Using indium as a surfactant during growth of the barriers by PAMBE, we were able to observe for the first time ISBA in strain-balanced m-plane AlGaN/InGaN superlattices.[19] Fig. 3(c) shows the ISBA spectra taken using the ATR-FTIR technique for a set of representative samples (A-C) with structural parameters detailed in the table shown in Fig. 3. The measured ISBA spans the mid-infrared 3.4-5.1 μm range, and exhibits linewidths comparable with the narrowest reported linewidths for indium-free m-plane QWs.[30-32] The direct- and ATR-FTIR measurements show the same expected dependence on QW width, charge density, and barrier Al composition. However, the ATR-FTIR technique consistently produces lower transition energies likely due to less distortion of the spectrum in the substrate. Calculations of the ISBA energies show that they are extremely sensitive to the choice of CBO. Conventional CBO values based on c-plane nitride measurements indicate that the LDA is more suitable for reproducing experimental transition values than the HFA. Overall, the LDA corrections slightly underestimates the ISB energies, but the remaining energy difference from experimental values can be easily compensated by a moderate increase of the CBO. The ISB transition energies achievable with AlGaN/$In_{0.16}Ga_{0.84}N$ superlattices do not reach the desirable near-infrared range below 3 μm. Therefore, additional research is needed to further increase the CBO. Since material issues related to m-plane AlGaN inhomogeneity at high aluminum composition are difficult to circumvent, CBO can mainly be increased by increasing the In-composition in the InGaN wells.

Sample	XRD thickness (nm)		In% QW/Barrier	Al%
	QW	Barrier		
A	2.8	7.5	15.5/5.6	19.2
B	2.8+1.25	7.2	16	21
C	3.4	5.8	15.5/0.4	24

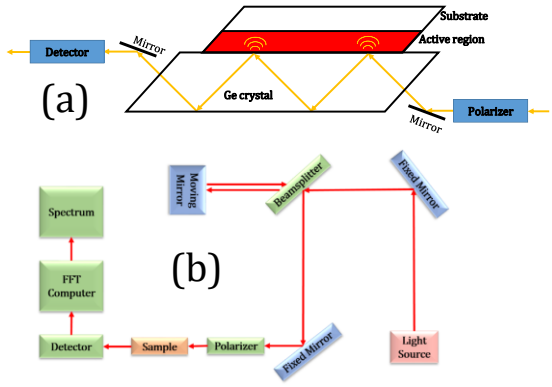

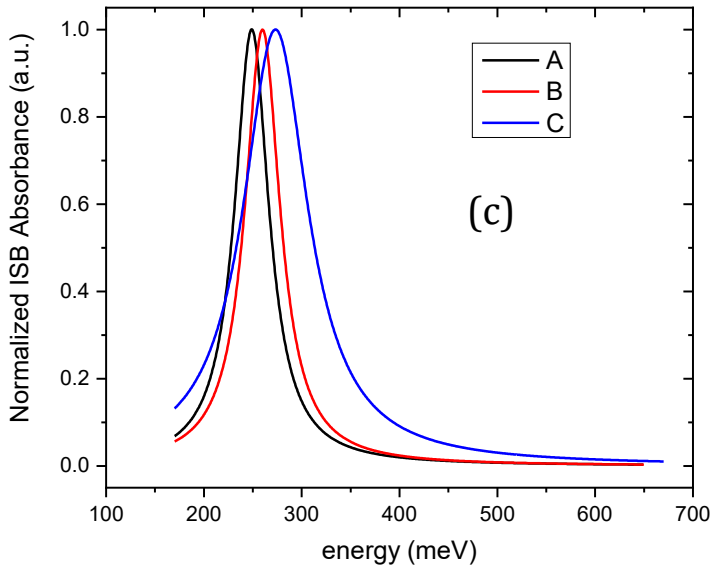

Figure 3. (a) Schematic of light propagation through the sample for ATR-FTIR measurement of ISBA. (c) General layout of ISBA measurements. (c) ATR-FTIR spectra of ISBA measured in three sample A-C with structural parameters summarized in the table.

4. PHOTOLUMINESCENCE

PL investigation of m-plane InGaN thin films grown by PAMBE indicated that the PL intensity at 80 K decreases dramatically for indium composition above 16% likely due to rapidly increasing density of non-radiative centers.[33] Therefore, PL measurements focused on nearly strain-balanced m-plane $In_xGa_{1-x}N/Al_yGa_{1-y}N$ (x = 0.09-0.16, $y \approx 0.2$) multi-QWs. Fig. 4(a) shows the steady-state PL at 80 K for three superlattices with nominally identical structural parameters that differ only in the conditions of barrier growth. We found that the use of an indium surfactant during barrier growth drastically increases PL intensity and decreases PL FWHM.[17] The FWHM decrease is attributed to a reduction of inhomogeneous broadening following significant improvement of AlGaN alloy uniformity.

An in-depth comparative study of undoped and doped m-plane InGaN/AlGaN superlattices was subsequently performed using continuous-excitation PL and time-resolved photoluminescence (TRPL). We found that the experimental steady-state PL energies of m-plane InGaN/AlGaN superlattices are systematically lower than the calculations made using generally accepted material parameters.[33] For example, the experimental PL peaks at 8 K are 3.095 eV for an undoped sample and 3.079 eV for a doped sample, while the calculated PL energies are 3.299 eV and 3.302 eV, respectively. The discrepancy was attributed to inhomogeneous distribution of In composition,[33] but may also be due to inaccurate deformation potential used to calculate strain effects in the simulation, or to other excitonic effects that were not included in the calculation. We note that at 80 K, the average PL degree of polarization for both samples is about 81%, which agrees with previous reports.[34]

It is generally accepted that the PL signal at low temperature is due to recombination of localized excitons. We have already reported the "S-shape" dependence of the PL peak position as a function of temperature that is typically associated with exciton localization.[33] Exciton localization in nonpolar InGaN/GaN QWs was attributed to strong hole localization at indium-rich fluctuations in the quantum wells. In the absence of intrinsic and piezoelectric fields on the m-plane, the electrons are no longer localized by well-width fluctuations, but are bound by Coulomb interaction to the localized holes. Therefore, it is likely that in our nearly strain-balanced superlattices, indium-rich regions are the main source of localization centers. The temperature dependence of PL FWHM allowed us to estimate an average localization depths of 21 meV and 40 meV for the undoped and doped structures, respectively. These values are smaller than previously reported for m-plane InGaN/GaN QWs grown by MOCVD.[35]

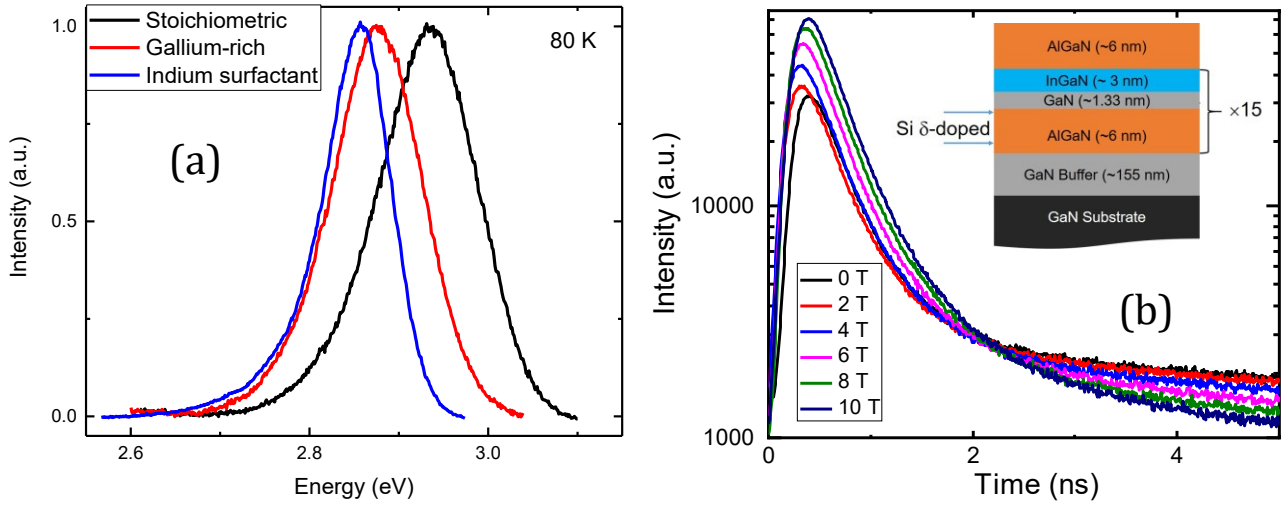

Figure 4. (a) PL of three undoped strain-balanced m-plane $In_{0.16}Ga_{0.84}N/Al_{0.2}Ga_{0.8}N$ multi-QW samples grown under different conditions. All spectra were scaled to a maximum of one. (b) TRPL of undoped strain-balanced m-plane $In_{0.09}Ga_{0.91}N/Al_{0.19}Ga_{0.81}N$ multi-QWs as a function of magnetic field at 2 K.

Temperature and magnetic-field dependence of TRPL was performed to examine carrier recombination and localization in m-plane strain-balanced $In_{0.09}Ga_{0.91}N/Al_{0.19}Ga_{0.81}N$ superlattices. Fig. 4(b) shows the TRPL of an undoped sample at 2 K for different magnetic fields. TRPL measurements in the temperature range 2 - 100 K identified two decay time scales for the undeped superlattice. At 2 K, the fast decay time τ_1 is 0.330±0.002 ns, while the slow decay time τ_2 is 2.18±0.06 ns, approximately 7 times longer than the initial fast decay time. The origin of these two time decays is not completely

understood at this point, but we attribute them to dual localization centers. In contrast, only one decay time (τ= 0.283±0.002 ns), and associated type of localization centers were found in doped structures. The localization centers characterized by sub-nanosecond time constants are likely due to indium fluctuations in the QWs, while those characterized by a nanosecond decay time are likely due to alloy inhomogeneity in the barriers. We attribute the absence of the second decay pathway in doped samples to a blocking effect of the doping sheets. The temperature dependence of the time constant allowed us to estimate the density of localization centers in undoped samples as 6×10^{12} cm^{-2}. Furthermore, TRPL indicates that at the lowest temperatures, carrier localization in the QWs is insensitive to magnetic field. In contrast, the decay time of excitons localized by barrier fluctuations decreases with increasing magnetic field.

5. CONCLUSIONS

Optical investigation with PL and ISBA measurements of strain-balanced nonpolar m-plane InGaN/AlGaN superlattices grown by PAMBE demonstrated that this material system is a viable alternative to traditional polar nitride heterostructures for optoelectronics and quantum sensing in the infrared. Careful optimization of the PAMBE process, in particular the use of an indium surfactant during barrier growth, has allowed us to overcome the intrinsic growth instability of m-plane AlGaN, and enabled growth of relatively homogeneous AlGaN barriers with sharp hetero-interfaces. These superlattices exhibit infrared ISB transitions in the 3.4-5.1 μm range that are well reproduced by band structure calculations corrected for many-body effect with the local-density approximation method. However, additional research is needed to extend their operation into the near-infrared. Further progress will require increasing the indium composition in the QWs above 16% and reducing InGaN localization center and non-radiative center densities.

ACKNOWLEDGEMENTS

We acknowledge support from the National Science Foundation. YC, TN, and OM acknowledge partial support from NSF award DMR-1610893, and DMR-2004462. AS and BD were supported from NSF award ECCS-1607173. GAK and BAM acknowledge the support from AFOSR under Grant FA9550-17-1-0341. A portion of this work was performed at the National High Magnetic Field Laboratory, which is supported by the National Science Foundation Cooperative Agreement No. DMR-1644779 and the State of Florida.

REFERENCES

[1] S. Nakamura, M. Senoh, N. Iwasa, and S.-I. Nagahama, Jpn. J. Appl. Phys. 34, L797 (1995).
[2] S. Nakamura, J. Vac. Sci. Tech. A 13, 705-710 (1995).
[3] S. Nakamura, T. Mukai, and M. Senoh, J. Appl. Phys. 76, 8189-8191 (1994).
[4] S. Nakamura, Microelectronics J. 25, 651-659 (1994).
[5] T. D. Moustakas, and P. Paiella, Rep. Prog. Phys. 80, 106501 (2017).
[6] D. Feezell, Y. Sharma, and S. Krishna, J. Appl. Phys. 113, 1133103 (2013).
[7] M. Beeler, E. Trichas, and E. Monroy, Semicond. Sci. Technol. 28, 074022 (2013).
[8] J. Wu, J. Appl. Phys. 106, 011101 (2009).
[9] C. Edmunds, L. Tang, D. Li, M. Cervantes, G. Gardner, T. Paskova, M. J. Manfra, and O. Malis, J. Electron. Matter. 41, 881 (2012).
[10] C. Edmunds, L. Tang, J. Shao, D. Li, M. Cervantes, G. Gardner, D. N, Zakharov, M. J. Manfra, and O. Malis, Appl. Phys. Lett. 101, 102104 (2012).
[11] J. Shao, D. Zakharov, C. Edmunds, O. Malis, and M. J. Manfra, Appl. Phys. Lett. 103, 232103 (2013).
[12] J. Shao, L. Tang, C. Edmunds, G. Gardner, O. Malis, and M. J. Manfra, J. Appl. Phys. 114, 023508 (2013).
[13] C. Edmunds, J. Shao, M. Shirazi-HD, M. J. Manfra, and O. Malis, Appl. Phys. Lett. 105, 021109 (2014).
[14] M. Shirazi-HD, R. E Diaz, T. Nguyen, J. Jian, G. C. Gardner, H. Wang, M. J. Manfra, and O. Malis, J. Appl. Phys. 123, 161581 (2018).
[15] T. Nguyen, M. Shirazi-HD, Y. Cao, R. E Diaz, G. C. Gardner, M. J. Manfra, and O. Malis, Phys. Status Solidi A 215, 1700828 (2018).
[16] A. Senichev, B. Dzuba, T. Nguyen, Y. Cao, M. A. Capano, M. J. Manfra, and O. Malis, APL Material. 7, 121109 (2019).

[17] B. Dzuba, A. Senichev, T. Nguyen, Y. Cao, R. E. Diaz, M. J. Manfra, and O. Malis, J. Appl. Phys. 128, 115701 (2020).
[18] B. Dzuba, T. Nguyen, Y. Cao, R. E. Diaz, M. J. Manfra, and O. Malis, J. Appl. Phys. 130, 105702 (2021).
[19] T. Nguyen, B. Dzuba, Y. Cao, A. Senichev, R. E Diaz, M. J. Manfra, and O. Malis, Optical Materials Express 11, 3284 (2021).
[20] S. Birner, T. Zibold, T. Andlauer, T. Kubis, M. Sabathil, A. Trellakis, and P. Vogl, IEEE Trans. Electron. Devices 54, 2137 (2007).
[21] I. Vurgaftman and J. R Meyer, J. Appl. Phys. 94, 3675-3696 (2003).
[22] T. Ando, Surface Science, 58(1), 128-134 (1976).
[23] S. J. Allen Jr., D. C. Tsui, and B. Vinter, Solid State Communication 20, 425-428 (1976).
[24] M. Helm, "The basic physics of intersubband transition," in Intersubband Transition in Quantum Wells: Physics and Device Applications I (Elsevier, 1999), Vol. 62, pp. 1-99.
[25] K. M. Bandara, D. D. Coon, O. Byungsung, Y. F. Lin, and M. H. Francombe, Appl. Phys. Lett. 53, 1931-1933, 1988.
[26] W. L. Bloss. J. Appl. Phys., 66(8), 3639-3642, 1989.
[27] L. Heldin and B. I. Lundqvist, J. Phys. C: Solid St. Phys. 4, 2064 (1971).
[28] K. M. Bandara, D. D. Coon, O. Byungsung, Y. F. Lin, and M. H. Francombe, "Erratum: Exchange interactions in quantum wells subbands," Appl. Phys. Lett. 55, 206 (1989).
[29] S. Schulz, D. P. Tanner, E. P. O'Reilly, M. A. Caro, T. L. Martin, P. A. J. Bagot, M. P. Moody, F. Tang, J. T. Griths, F. Oehler, M. J. Kappers, R. A. Oliver, C. J. Humphreys, D. Sutherland, M. J. Davies, and P. Dawson, Phys. Rev. B. 92, 235419 (2015).
[30] A. Pesach, E. Gross, C. -Y. Huang, Y. -D. Lin, S. E. Schacham, S. Nakamura, and G. Bahir, Appl. Phys. Lett. 103, 022110 (2013).
[31] T. Kotani, M. Arita, and Y. Arakawa, Appl. Phys. Lett. 105, 261108 (2014).
[32] T. Kotani, M. Arita, and Y. Arakawa, Appl. Phys. Lett. 107, 112107 (2015).
[33] Y. Cao, B. Dzuba, B. Magill, A. Senichev, T. Nguyen, R. Diaz, M. Manfra, S. McGill, C. Garcia, G. Khodaparast, and O. Malis, J. Appl. Phys. 127, 185702 (2020).
[34] S. Marcinkevičius, K. M. Kelchner, S. Nakamura, S. P. DenBaars, and J. S. Speck, Appl. Phys. Lett. 102, 101102 (2013).
[35] V. Liuolia, A. Pinos, S. Marcinkevičius, Y. D. Lin, H. Ohta, S. P. DenBaars, and S. Nakamura, Appl. Phys. Lett. 97, 151106 (2010).